


# Measurement of far-infrared surface phonon polaritons in AlN nanowires via electron microscope

Chao He(何超), Ze Hua(华泽), Peiyi He(何沛一), Ruishi Qi(亓瑞时), Yuehui Li(李跃辉), Ruiwen Shao(邵瑞文), Weikang Dong(董伟康), Ruochen Shi(时若晨), Yeliang Wang(王业亮), and Peng Gao(高鹏)

**Citation:**Chin. Phys. B, 2026, 35 (**3**): 037901. DOI: 10.1088/1674-1056/ae2a00
http://cpb.iphy.ac.cn; http://iopscience.iop.org/cpb

**What follows is a list of articles you may be interested in**

---

## Relation of V/III ratio of AlN interlayer with the polarity of nitride

Zhaole Su(苏兆乐), Yangfeng Li(李阳锋), Xiaotao Hu(胡小涛), Yimeng Song(宋祎萌), Zhen Deng(邓震), Ziguang Ma(马紫光), Chunhua Du(杜春花), Wenxin Wang(王文新), Haiqiang Jia(贾海强), Yang Jiang(江洋), and Hong Chen(陈弘)

Chin. Phys. B, 2024, 33 (**11**): 117801. DOI: 10.1088/1674-1056/ad71b2

## Electroluminescence explored internal behavior of carriers in InGaAsP single-junction solar cell

Xue-Fei Li(李雪飞), Wen-Xian Yang(杨文献), Jun-Hua Long(龙军华), Ming Tan(谭明), Shan Jin(金山), Dong-Ying Wu(吴栋颖), Yuan-Yuan Wu(吴渊渊), and Shu-Long Lu(陆书龙)

Chin. Phys. B, 2023, 32 (**1**): 017801. DOI: 10.1088/1674-1056/ac7448

## Enhanced absorption process in the thin active region of GaAs based p-i-n structure

Chen Yue(岳琛), Xian-Sheng Tang(唐先胜), Yang-Feng Li(李阳锋), Wen-Qi Wang(王文奇), Xin-Xin Li(李欣欣), Jun-Yang Zhang(张珺玚), Zhen Deng(邓震), Chun-Hua Du(杜春花), Hai-Qiang Jia(贾海强), Wen-Xin Wang(王文新), Wei Lu(陆卫), Yang Jiang(江洋), and Hong Chen(陈弘)

Chin. Phys. B, 2021, 30 (**9**): 097803. DOI: 10.1088/1674-1056/abf10c

## Magneto-optical properties of self-assembled InAs quantum dots for quantum information processing

Jing Tang(唐静), Xiu-Lai Xu(许秀来)

Chin. Phys. B, 2018, 27 (**2**): 027804. DOI: 10.1088/1674-1056/27/2/027804

## Thin film micro-scaled cold cathode structures of undoped and Si-doped AlN grown on SiC substrate with low turn-on voltage

Shi Ming (侍铭), Chen Ping (陈平), Zhao De-Gang (赵德刚), Jiang De-Sheng (江德生), Zheng Jun (郑军), Cheng Bu-Wen (成步文), Zhu Jian-Jun (朱建军), Liu Zong-Shun (刘宗顺), Liu Wei (刘炜), Li Xiang (李翔), Zhao Dan-Mei (赵丹梅), Wang Qi-Ming (王启明), Liu Jian-Ping (刘建平), Zhang Shu-Ming (张书明), Yang Hui (杨辉)

Chin. Phys. B, 2015, 24 (**5**): 057901. DOI: 10.1088/1674-1056/24/5/057901

---

**RAPID COMMUNICATION**

# Measurement of far-infrared surface phonon polaritons in AlN nanowires via electron microscope

Chao He(何超)[1,7], Ze Hua(华泽)[2], Peiyi He(何沛一)[3], Ruishi Qi(亓瑞时)[4], Yuehui Li(李跃辉)[3,5], Ruiwen Shao(邵瑞文)[2], Weikang Dong(董伟康)[6], Ruochen Shi(时若晨)[3,†], Yeliang Wang(王业亮)[1,‡], and Peng Gao(高鹏)[3,§]

[1] *School of Integrated Circuits and Electronics, Beijing Institute of Technology, Beijing* 100081, *China*
[2] *Beijing Advanced Innovation Center for Intelligent Robots and Systems and School of Medical Technology, Beijing Institute of Technology, Beijing* 100081, *China*
[3] *International Center for Quantum Materials and Electron Microscopy Laboratory, School of Physics, Peking University, Beijing* 100871, *China*
[4] *Physics Department, University of California at Berkeley, Berkeley, CA* 94720, *USA*
[5] *Institute of Quantum Materials and Physics, Henan Academy of Sciences, Zhengzhou* 450002, *China*
[6] *The Institute of Scientific and Industrial Research, The University of Osaka, Ibaraki, Japan*
[7] *Beijing Goldenscope Technology Co., Ltd., Beijing* 100096, *China*

(Received 11 October 2025; revised manuscript received 26 November 2025; accepted manuscript online 9 December 2025)

Surface phonon polaritons (SPhPs) exhibit promising advantages (e.g., low loss, long lifetimes) for mid/far-infrared (MIR/FIR) nanophotonics. However, FIR SPhPs experiments remain challenging for conventional optics and scattering-type scanning near-field optical microscopy (s-SNOM) due to the lack of compatible light sources/detectors. In this work, we characterized ∼ 75–110 meV SPhPs in AlN nanowires using a monochromated scanning transmission electron microscope (STEM) equipped with electron energy loss spectroscopy (EELS). This technique provided exceptional 4.3 meV energy resolution and sub-angstrom spatial resolution. We observed the evolution of SPhP interference fringes with propagation distance, derived the dispersion curve, and clarified size effects on SPhP propagation by tuning AlN structure dimensions. Experimental-numerical cross-validation confirmed that the local continuum model (LCM) accurately describes AlN's SPhP behaviors. This work advances the understanding of FIR SPhPs in polar dielectrics and establishes a robust platform for studying FIR phonon polariton materials.

**Keywords:** AlN, surface phonon polaritons (SPhPs), far-infrared, STEM-EELS, nanowires

**PACS:** 79.20.Uv, 78.55.Cr

**DOI:** 10.1088/1674-1056/ae2a00 **CSTR:** 32038.14.CPB.ae2a00

## 1. Introduction

Surface phonon polaritons (SPhPs) are electromagnetic surface waves arising from the coupling of photons with transverse-optical (TO) phonons.[1,2] Within the Reststrahlen band — bounded by the TO and longitudinal optical (LO) phonon frequencies of polar dielectrics — SPhPs are sustained via the interaction between incident light and oscillating ionic charges in the polar lattice.[1,3] A key advantage of SPhPs over surface plasmon polaritons (SPPs) is their significantly lower propagation loss.[4] For SPPs, the high optical losses, primarily induced by electron scattering, limit their performance as low-dimensional electromagnetic energy carriers.[5–7] These inherent losses of SPPs, which restrict their practical utility, underscore the need for alternative light-confining mechanisms.[3] This makes low-loss SPhPs a highly attractive alternative.[6,8–11]

Conventional techniques for characterizing SPhPs, including infrared absorption spectroscopy,[12] Raman scattering spectroscopy,[13] and inelastic x-ray scattering,[14] suffer from low spatial resolution, rendering them unsuitable for nanophotonic research. While scattering-type scanning near-field optical microscopy (s-SNOM) has been employed to study mid-infrared (MIR) SPhPs in materials such as $MoO_3$[15] and h-BN,[16] it is typically limited to two spectral windows: the near-mid-infrared ($>$ 100 meV) and terahertz ($<$ 10 meV) ranges.[17] Notably, most polar materials support SPhPs in the far-infrared (FIR) region (10–100 meV); however, investigations in this range have long been constrained by the lack of commercially suitable light sources and detectors. To our knowledge, the absence of high-spatial-resolution studies in this critical spectral window has hindered both a comprehensive understanding of SPhP properties and the exploration of new SPhP-supporting materials, thus constrained progress in advancing FIR polaritonic technologies.

Recent advances in scanning transmission electron

†Corresponding author. E-mail: shirc1993@pku.edu.cn
‡Corresponding author. E-mail: yeliang.wang@bit.edu.cn
§Corresponding author. E-mail: pgao@pku.edu.cn

© 2026 Chinese Physical Society and IOP Publishing Ltd. All rights, including for text and data mining, AI training, and similar technologies, are reserved.

microscopy (STEM) equipped with electron energy loss spectroscopy (EELS) have addressed this gap, enabling SPhP characterization with both high spatial and energy resolution.[4,17,18] State-of-the-art modern STEM systems are equipped with a monochromator and an ultra-bright cold-field emission electron gun (CFEG). The CFEG provides a narrow electron beam with high brightness, ensuring exceptional imaging resolution.[19–21] Concurrently, the monochromator effectively reduces energy spread of the electron source, enhancing energy coherence.[22–24] This high energy resolution, reaching up to sub-10 meV, allows us to distinguish higher-order SPhP modes and elucidate fundamental physical properties.

This study focuses on aluminum nitride (AlN), a prototypical bulk polar crystal that supports SPhPs in the near-MIR-to-FIR range, with high academic and application value. AlN is highly compatible with mainstream silicon-based semiconductor processes — its lattice matching, thermal stability, and inertness meet chip-level integration needs, laying a foundation for large-scale phonon polariton devices.[25,26] It also has a wide bandgap ($\sim$ 6.2 eV), which enables deep-ultraviolet (DUV) devices to show potential in sterilization and storage.[27] Harnessing SPhPs in AlN would expand DUV device functions, e.g., enhancing light field localization to boost response speed and efficiency.

We fabricated AlN nanowires of varying dimensions using a focused ion beam (FIB) system on ThermoFisher Helios G4, and then carefully characterized them using a Nion UltraSTEM 200 (with monochromator and aberration corrector). Our experiments revealed SPhP interference fringes, from which we derived the dispersion relation and clarified size-dependent propagation effects. Key observations included energy red-shifts with increasing structure length and the emergence of distinct corner and face modes in near-square nanowires. These findings were validated through electromagnetic simulations. This work provides fundamental insights into FIR SPhPs in a commercially vital semiconductor and establishes a robust framework for studying FIR phonon polariton materials.

## 2. Results and discussion

The complex dielectric function of the AlN lattice can be expressed as

$$\varepsilon = \varepsilon_\infty + \frac{S\omega_{\mathrm{TO}}^2}{\omega_{\mathrm{TO}}^2 - \omega^2 - \mathrm{i}\Gamma\omega}, \tag{1}$$

where $\omega$ is the frequency of the incident electric field, and $\Gamma$ is the damping constant. $\varepsilon_\infty$ is the high frequency limit of the dielectric function, $S$ is the oscillator strength, $S = \varepsilon_0 - \varepsilon_\infty$, and $\varepsilon_0$ is the low frequency limit of the dielectric function.

Using Eq. (1), we calculated the complex dielectric function of AlN. As shown in Fig. 1, the real (Re($\varepsilon$), red curve) and imaginary (Im($\varepsilon$), blue curve) parts of the dielectric function define the Reststrahlen band, which lies between the transverse optical (TO) and longitudinal optical (LO) phonon frequencies — marked by the onset and end of the yellow shaded region, respectively. For AlN, this band spans from $\omega_{\mathrm{TO}} = 76.1$ meV to $\omega_{\mathrm{LO}} = 108.5$ meV.[28] The other parameters used in dielectric function calculation include $\Gamma = 2.5$ meV, $\varepsilon_\infty = 5.36$ and $S = 1.03$. We note that AlN exhibits a slight anisotropy in its dielectric properties. However, given that the reported anisotropy in the dielectric constants is only about 3.5%,[28] and considering that the SPhPs investigated herein primarily propagate along the $c$-axis ([0001] direction) of the nanowires, we have utilized the dielectric parameters for the $c$-axis parallel polarization to calculate the permittivity for our simulations and analysis. The inset in Fig. 1 schematically illustrates the atomic structure of AlN.

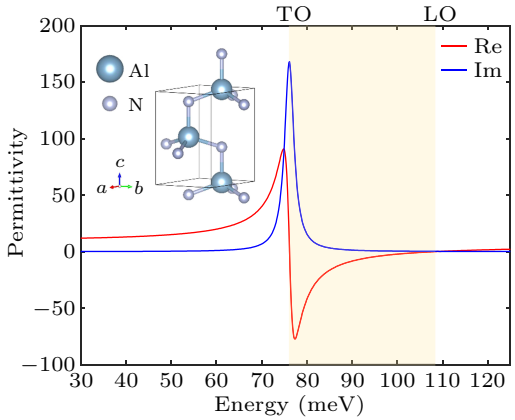



**Fig. 1.** Complex permittivity of AlN. The real (red) and imaginary (blue) parts of complex permittivity are plotted. The light-yellow shaded region denotes the Reststrahlen band, with its edge corresponding to the TO and LO phonon energies respectively. The inset illustrates the atomic structure of AlN.

Achieving high energy resolution is paramount for resolving the fine spectral features of SPhPs. As the acceleration voltage is a critical factor determining energy resolution, we performed the EELS measurement at 30 kV, rather than the conventional 60 kV. The comparison of typical zero-loss peak (ZLP) for 30 kV and 60 kV is shown in Fig. 2(a). The ZLP at 30 kV is significantly sharper, with its full width at half maximum (FWHM) narrowing from 10 meV at 60 kV to 4.3 meV. This corresponds to a factor of two improvement in energy resolution. Furthermore, the measurement at 30 kV exhibited a superior signal-to-noise ratio, higher peak intensity, and improved peak sharpness (Fig. 2(a), insets).

Leveraging this high resolution, we characterized SPhPs in AlN nanowires fabricated via focused ion beam (FIB) with their long axis aligned along the [0001] direction of AlN and the width direction along the [10-10] direction. The electron beam was incident along the thickness direction of the nanowire. The high-angle annular dark field (HAADF) image of a representative structure with dimensions of 2000 nm (length) $\times$300 nm (width) $\times$270 nm (thickness) is shown in

Fig. 2(b). We acquired electron energy-loss spectra by scanning the electron beam vertically along the nanowire's long side (colored arrow). Notably, when the electron beams pass through the vicinity of the nanowire without direct intersecting, SPhPs can still be excited and well detected due to the long-range Coulomb interaction. This measurement method is called the aloof mode, which is frequently used in EELS studies.[29] After background subtraction and normalization, the resulting spectrum (Fig. 2(c)) revealed multiple peaks. The spatial position of each spectrum corresponds to the location of the same color along the arrow in Fig. 2(b). The distance from the bottom end of the nanowire (defined as positive upwards) is encoded in the color, as indicated by the color bar above the panel. Among these, one peak exhibited significant variations in both energy and intensity with changing beam position. A prominent peak shift of this peak was observed across the 77 meV to 102 meV range, which we attribute to the SPhP dispersion.

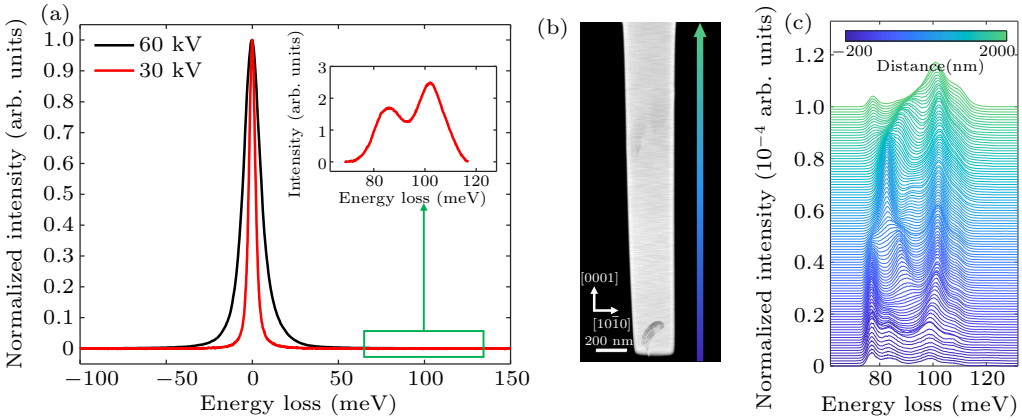



**Fig. 2.** Measurement of phonon polaritons in an AlN nanowire at 30 kV. (a) Comparison of the zero-loss peaks (ZLP) at 30 kV (red) and 60 kV (black). The FWHMs of 30 kV and 60 kV are labeled by horizonal bars. The AlN phonon polariton signal is circled (green box) and enlarged as the inset. (b) HAADF image of the fabricated AlN nanowire. The colored line marks the path of the EELS line scan. (c) EELS intensity map along the nanowire, color-coded according to the spatial position shown in the top bar. The pronounced energy shift of one peak identifies it as a surface phonon polariton.

In order to investigate the properties of SPhPs in detail, Fig. 3 presents the spatial-and-energy-resolved EELS measurement of the same nanowire in Fig. 2. The experimental two-dimensional EELS mapping at different energies is given in Fig. 3(a). The signal is strongest at the ends of the nanowire, similar to the properties of SPPs. The observed interference fringes result from SPhPs excited by the beam and propagating along the nanowire, as shown in Fig. 3(b). For the propagating SPhPs, the increasing distance of the interference fringes from the nanowire ends corresponds to a longer wavelength and thus a smaller wavenumber. Experimentally, as the electron beam moves from the center towards the ends of the nanowire, the wavenumber increases, and the energy of the most intense mode gradually rises, consistent with the lower-branch SPhP dispersion relation.[4,17] In addition to these dispersive, propagating SPhPs, we also identified several non-dispersive SPhP modes along the nanowire axis. The mode at 102 meV is identified as a radially propagating SPhP, while the modes at 78 meV and 84 meV, which are significantly enhanced near the nanowire ends, are resonant dipolar modes with different wavevectors propagating along the nanowire edges. When approaching the end of nanowire, these non-dispersive modes also exhibit slight energy shifts and peak broadening. This is because their energies become very close to those of other multipolar modes at the end, convoluting into a single, spectrally unresolved broad peak. These phenomena are highly consistent with the observations reported in previous study.[30] The slight asymmetry in the SPhP signal intensity along the nanowire's long axis is attributed to the influence of the residual bulk AlN base, which was retained at one end for structural support during the FIB fabrication process.

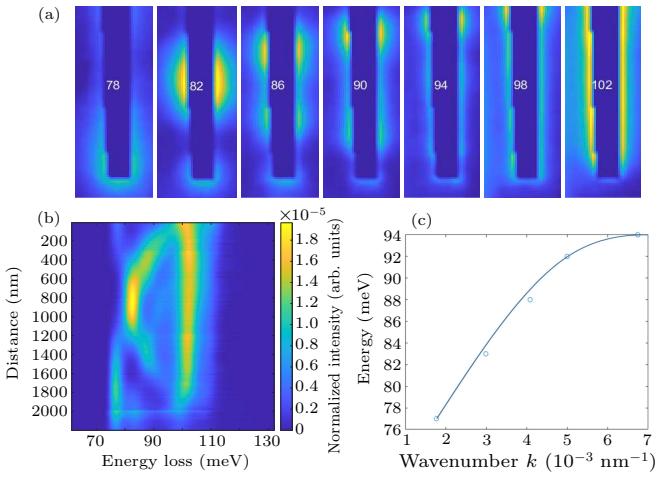



**Fig. 3.** The spatial-and-energy-resolved EELS measurement of AlN nanowire. (a) Experimental 2D EELS maps around the nanowire, showing interference fringes from propagating SPhPs at different energies. (b) EELS line profile along longitudinal axis of the nanowire. (c) Experimental SPhP dispersion relation (energy as a function of the wavenumber $k$) extracted from the fringe period (blue circle), compared with the theoretical model (dark blue line).

For the peak spanning 77–102 meV, its pronounced energy shift indicates a strong dispersion relation. Therefore,

we calculated the dispersion relation to elucidate this behavior. The dispersion relation can be derived from Maxwell's equations as

$$v'\epsilon\frac{\mathrm{d}\ln I_0(vl)}{\mathrm{d}(vl)} = v\frac{\mathrm{d}\ln K_0(v'l)}{\mathrm{d}(v'l)}, \tag{2}$$

where $\epsilon = \epsilon(\omega)$ is the frequency-dependent permittivity of AlN, $v = \sqrt{k^2 - \epsilon\omega^2/c^2}$, $v' = \sqrt{k^2 - \omega^2/c^2}$, $c$ is the speed of light in vacuum, $l$ is the length of the nanowire, $k$ is the wavevector, $\omega$ is the vibrational frequency, and the functions $I_0$ and $K_0$ are the modified Bessel functions of the first and second kind of order zero, respectively. Although this analytical expression is derived for cylindrical nanowires, it is employed here as a close approximation for the dispersion relations in our rectangular nanowires, justified by their comparable width and thickness and the corner rounding induced by the FIB fabrication process.

In Fig. 3(c), the theoretical dispersion curve is plotted in dark blue line, and the blue circles represent the wavevector-energy ($k$–$E$) pairs extracted from our experimental data. The experimental dispersion is in good agreement with the theoretical model of Eq. (2). The minor discrepancies are primarily attributed to the small energy differences ($< 2$ meV) between multiple eigen modes, which are challenging to resolve experimentally. The remarkable agreement between experiment and theory confirms the validity of using the analytical model for cylindrical nanowires to approximate the SPhP dispersion in our fabricated nanostructures.

To study the influence of geometric dimensions on SPhPs, we fabricated the nanowires of alternative dimensions (length: 1150 nm, width: 450 nm, thickness: 450 nm) using identical methods. Figure 4(a) displays the HAADF image of the nanowire and experimental 2D EELS mapping at different energies. The corner mode at 84 meV and the edge mode at 88 meV are observed. For clarity, the EELS spectra line profiles along the vertical and horizontal directions are plotted in Figs. 4(b) and 4(c), respectively. Along the vertical direction (Fig. 4(b)), a corner mode appears at 93 meV near the two ends (0–200 nm and 900–1100 nm). Besides, an edge mode emerges at 100 meV. The propagating SPhPs are observed between 94–99 meV. Compared with the data in Fig. 3(b), it exhibits a smaller energy shift range, indicating its weaker propagation, likely due to the shorter nanowire length. In the horizontal direction at the front end of the nanowire (Fig. 4(c)), both the corner mode (93 meV) and the edge mode (100 meV) are present within the same energy interval. However, SPhP propagation is hardly observable. The stark contrast between the vertical and horizontal energy distributions underscores a significant size effect.

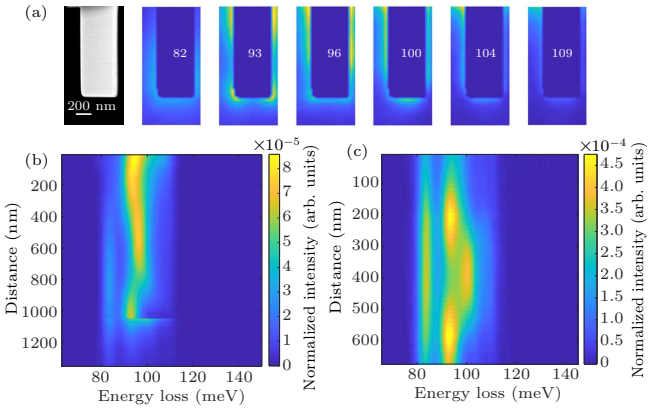



**Fig. 4.** SPhPs in a 1150 nm × 450 nm AlN nanowire. (a) HAADF and 2D EELS mapping. (b)–(c) EELS line profile along vertical direction (b) and horizontal direction (c). The corner mode ∼ 93 meV and edge mode ∼ 100 meV are observed. The difference in SPhP propagation between the vertical and horizontal energy distributions reveals a pronounced size effect.

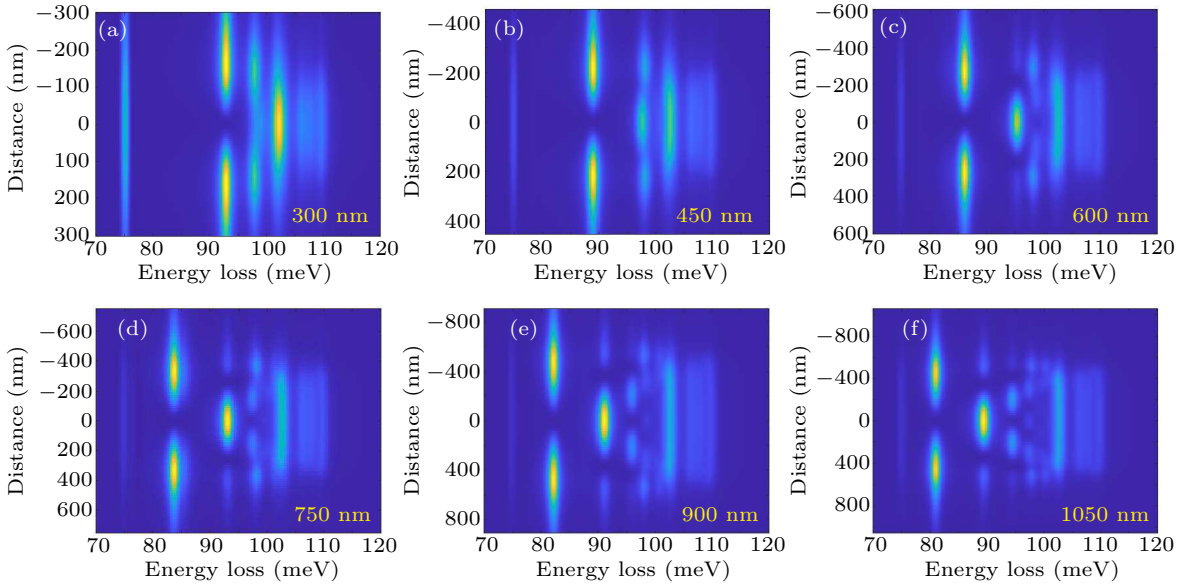



**Fig. 5.** Simulated EELS spectra for AlN nanowires of varying lengths. The lengths of nanowires are (a) 300 nm, (b) 450 nm, (c) 600 nm, (d) 750 nm, (e) 900 nm, and (f) 1050 nm, respectively. The width of nanowires is fixed at 300 nm. A red-shift of the dipole mode is observed with increasing nanowire length.

To systematically study this size effect on SPhP propagation, we performed numerical simulations using the boundary element method (BEM)[31] based on a local continuum model, an established approach for solving Maxwell's equations in such systems.[32] Figure 5 shows the simulated spatial-energy distribution for AlN nanowires of varying lengths (from 300 nm to 1050 nm) at a fixed width of 300 nm. The simulations confirm that the dipole mode of the nanowire exhibits a red shift with increasing nanowire length. This phenomenon agrees well with the experimental results. These results demonstrate that structural dimensions are a highly effective means to control SPhP propagation.

## 3. Conclusion

In summary, this study investigated the SPhPs of AlN nanowires and their correlation with the geometric dimensions of individual AlN nanowires. Through experiments and simulations, we elucidated the size effect on SPhPs. Notably, we demonstrated that the propagation length and energy of SPhPs are highly sensitive to the nanostructure's length, while the aspect ratio governs the transition from propagating to localized modes (e.g., corner and edge modes). These results not only advance the understanding of SPhP behavior at the nanoscale but also provide foundational insights for the rational design of related polaritonic technologies. Additionally, the state-of-the-art STEM-EELS with atomic spatial resolution and 4 meV energy resolution opens new opportunities to explore fundamental physical excitations across a broad energy range.

## Acknowledgements

The work was supported by the National Key R&D Program of China (Grant No. 2023YFB3609903), the National Natural Science Foundation of China (Grant Nos. 52125307 and 12404192), the "2011 Program" from the Peking–Tsinghua–IOP Collaborative Innovation Center of Quantum Matter. P.G. acknowledges the support from the New Cornerstone Science Foundation through the XPLORER PRIZE. We acknowledge Electron Microscopy Laboratory of Peking University for the use of electron microscopes. We acknowledge High-performance Computing Platform of Peking University for providing computational resources.

## References

[1] Yu P Y and Cardona M 2010 *Fundamentals of Semiconductors: Physics and Materials Properties* (Berlin, Heidelberg: Springer)
[2] Ayari A, Cobas E, Ogundadegbe O and Fuhrer M S 2007 *J. Appl. Phys.* **101** 014507
[3] Karakachian H and Kazan M 2017 *J. Appl. Phys.* **122** 045103
[4] Li Y, Qi R, Shi R, Li N and Gao P 2020 *Science Bulletin* **65** 820
[5] Boltasseva A and Atwater H A 2011 *Science* **331** 290
[6] Khurgin J B and Sun G 2011 *Appl. Phys. Lett.* **99** 211106
[7] West P R, Ishii S, Naik G V, Emani N K, Shalaev V M and Boltasseva A 2010 *Laser & Photonics Reviews* **4** 795
[8] Khurgin J B 2015 *Nat. Nanotech.* **10** 2
[9] Caldwell J D, Lindsay L, Giannini V, Vurgaftman I, Reinecke T L, Maier S A and Glembocki O J 2015 *Nanophotonics* **4** 44
[10] Caldwell J D, Vurgaftman I, Tischler J G, Glembocki O J, Owrutsky J C and Reinecke T L 2016 *Nat. Nanotech.* **11** 9
[11] Li N, Guo X, Yang X, Qi R, Qiao T, Li Y, Shi R, Li Y, Liu K, Xu Z, Liu L, García De Abajo F J, Dai Q, Wang E G and Gao P 2021 *Nat. Mater.* **20** 43
[12] Anderson M S 2005 *Appl. Phys. Lett.* **87** 144102
[13] Efremov E V, Ariese F and Gooijer C 2008 *Analytica Chimica Acta* **606** 119
[14] Le Tacon M, Bosak A, Souliou S M, Dellea G, Loew T, Heid R, Bohnen K P, Ghiringhelli G, Krisch M and Keimer B 2014 *Nat. Phys* **10** 52
[15] Ma W, Alonso-González P, Li S, Nikitin A Y, Yuan J, Martín-Sánchez J, Taboada-Gutiérrez J, Amenabar I, Li P, Vélez S, Tollan C, Dai Z, Zhang Y, Sriram S, Kalantar-Zadeh K, Lee S T, Hillenbrand R and Bao Q 2018 *Nature* **562** 557
[16] Xu X G, Ghamsari B G, Jiang J H, Gilburd L, Andreev G O, Zhi C, Bando Y, Golberg D, Berini P and Walker G C 2014 *Nat. Commun.* **5** 4782
[17] Qi R, Wang R, Li Y, Sun Y, Chen S, Han B, Li N, Zhang Q, Liu X, Yu D and Gao P 2019 *Nano Lett.* **19** 5070
[18] Dong W, Qi R, Liu T, Li Y, Li N, Hua Z, Gao Z, Zhang S, Liu K, Guo J and Gao P 2020 *Adv. Mater.* **32** 2002014
[19] Ruben G, Bosman M, D'Alfonso A J, Okunishi E, Kondo Y and Allen L J 2011 *Ultramicroscopy* **111** 1540
[20] Bowman W J, March K, Hernandez C A and Crozier P A 2016 *Ultramicroscopy* **167** 5
[21] James E M and Browning N D 1999 *Ultramicroscopy* **78** 125
[22] Krivanek O L, Ursin J P, Bacon N J, Corbin G J, Dellby N, Hrncirik P, Murfitt M F, Own C S and Szilagyi Z S 2009 *Phil. Trans. R. Soc. A* **367** 3683
[23] Krivanek O L, Lovejoy T C, Murfitt M F, Skone G, Batson P E and Dellby N 2014 *J. Phys.: Conf. Ser.* **522** 012023
[24] Kimoto K 2014 *Microscopy (Tokyo)* **63** 337
[25] Paudel T R and Lambrecht W R L 2009 *Phys. Rev. B* **80** 104202
[26] Xu Z, Zhang Y, Shen J, Dong Y, Wu L, Xu J and Su Y 2022 *Opt. Lett.* **47** 4925
[27] Li N, Ho C P, Zhu S, Fu Y H, Zhu Y and Lee L Y T 2021 *Nanophotonics* **10** 2347
[28] Bungaro C, Rapcewicz K and Bernholc J 2000 *Phys. Rev. B* **61** 6720
[29] Crozier P A 2017 *Ultramicroscopy* **180** 104
[30] He P, Li J, Li C, Li N, Han B, Shi R, Qi R, Du J, Yu P and Gao P 2025 *Sci. Adv.* **11** eady7316
[31] Hohenester U 2014 *Comput. Phys. Commun.* **185** 1177
[32] Lourenço-Martins H and Kociak M 2017 *Phys. Rev. X* **7** 041059